Journal of Materials Chemistry B

ROYAL SOCIETY OF CHEMISTRY

PAPER

View Article Online
View Journal | View Issue

Cite this: J. Mater. Chem. B, 2022, 10, 2584

Bio-inspired antibacterial coatings on urinary stents for encrustation prevention†

Qin Yao,‡[a] Binghai Chen,‡[a] Jiaxiang Bai,*[b] Wenbo He,[c] Xu Chen,[c] Dechun Geng*[b] and Guoqing Pan*[c]

Received 22nd October 2021,
Accepted 20th December 2021

DOI: 10.1039/d1tb02318g

rsc.li/materials-b

Urinary tract infection (UTI) represents one of the most common nosocomial infections, which is mainly related to indwelling catheters or stents. In addition to the formation of biofilms to reduce antibiotic sensitivity, the urease-producing bacteria can also increase urine pH, causing Ca^{2+} and Mg^{2+} deposition and finally catheter obstruction. The prevention of UTIs and its complication (*i.e.*, encrustation) thus is a great challenge in design of catheters and ureteral stents. In this work, a metal-catechol-assisted mussel chemistry (*i.e.*, dopamine self-polymerization) was employed for surface functionalization of commercially available catheters with antimicrobial peptides (AMP), for the purpose of long-term anti-infection and encrustation prevention. To improve the stability of the polydopamine coating on polymeric stents, we used Cu^{2+}-coordinated dopamine self-polymerization. Then, a cysteine-terminated AMP was introduced on the polydopamine coating through Michael addition. We found that the Cu^{2+}-coordinated polydopamine coating showed improved stability and antibacterial effect. The cytotoxicity test confirmed that the bioinspired antibacterial coating showed good biocompatibility and no obvious toxicity. The results confirmed that the stents with AMP could *in situ* inhibit bacterial growth and biofilm formation, and finally reduce the deposition of struvite and hydroxyapatite crystals both *in vitro* and *in vivo*. We anticipate that this bioinspired strategy would develop a safe, stable and effective antibacterial coating on urinary tract medical devices for long-term bacterial inhibition and encrustation prevention.

1. Introduction

Catheters and ureteral stents are among the most commonly used medical devices in patients with urologic disorders.[1,2] Currently, various polymeric materials including polyurethane (PU), silicone, polytetrafluoroethylene (PTFE), polyvinylchloride (PVC), and latex rubber have been widely employed to produce catheters/stents.[3,4] In clinics, the stents can be used for the treatment of typical urinary diseases like urinary tract obstruction, or for renal and ureteral surgery,[5] and the catheters are commonly used as an adjunct to relieve urinary incontinence and urinary retention as well as urinary diversion in bladder, prostate and urethral surgery. These devices have proven to be very effective in urinary drainage and supporting the urethra and ureters, but can also cause side effects for patients, such as discomfort, pain, haematuria, and in particular, chronic infection and subsequently encrustation.[6–9]

Long-term indwelling of the catheters or stents will inevitably lead to catheter associated urinary tract infections (UTIs).[10–13] When the catheter or stent is surgically inserted, it inevitably destroys the protective barrier of the urinary system, and the bacteria can follow the catheter/stent retrograde into the urinary system and cause infections.[14] In addition to the immediate harm of pathogens to patients, the infection can also induce chronic disease. Upon the surface attachment of bacteria, they begin to secrete an extracellular matrix, which enables the formation of a layer of biofilm on the surface of catheters/stents.[15,16] Biofilms can reduce the antibiotic sensitivity. In addition, several typical pathogens in the urinary system, including *Proteus mirabilis* (*P. mirabilis*), *Klebsiella pneumoniae* (*K. pneumoniae*) and *Pseudomonas aeruginosa* (*P. aeruginosa*), produce ureases that can decompose urea with a faster rate (6 to 25 times higher) than that of other enzymes.[17,18] Once excess urea was decomposed into ammonia, the pH value of urine would rapidly raise up to 8.5. In an

[a] Department of Urology, Affiliated Hospital of Jiangsu University, 438 Jiefang Road, Zhenjiang, Jiangsu, 212001, China. E-mail: jxbai1995@163.com, szgengdc@163.com
[b] Department of Orthopaedic Surgery, Orthopaedic Institute, The First Affiliated Hospital, Medical College, Soochow University, Suzhou, Jiangsu, 215006, China
[c] Institute for Advanced Materials, School of Materials Science and Engineering, Jiangsu University, 301 Xuefu Road, Zhenjiang, Jiangsu, 212013, China. E-mail: panguoqing@ujs.edu.cn

† Electronic supplementary information (ESI) available. See DOI: 10.1039/d1tb02318g

‡ These authors contributed equally to this work.

alkaline environment, calcium phosphate and magnesium would deposit and form insoluble struvite and hydroxyapatite.[4,6,19,20] Such infection-caused depositions on catheters or stents will eventually block the flow channels and cause obstruction. The depositions can gradually grow and lead to the failure of the catheters or stents. More seriously, endoscopic or open surgery may require removing the devices. Conceivably, UTIs and the complications have brought enormous burdens to patients. Current clinical treatments to ameliorate UTI mainly rely on antibiotics and regular catheter replacement. Leaving the pain caused by regular replacements aside, long-term administration of antibiotics will cause bacterial resistance, which may bring another trouble to the patients. In this context, the development of catheters/stents with antibiotic-free bactericidal ability and capability of *in situ* prevention of chronic UTIs and urinary encrustation is highly anticipated.

Antimicrobial peptides (AMPs) are a set of natural host defence peptides, first discovered in the study of ''why the moist surface of amphibians did not permanently infect''.[21] AMPs have been revealed with various functions, including behaving as immunomodulators to stimulate the accumulation of immune cells at the site of infection, controlling immune responses against a particular microorganism, showing anti-inflammatory properties, neutralizing endotoxins produced by bacteria, stimulating angiogenesis, and accelerating wound repair. Different from antibiotics with specific target molecules (*e.g.*, peptides, proteins and DNAs), AMPs target the lipopolysaccharide layer of the cell membrane due to their unique structure of cationic and amphipathic residues. The membrane permeabilization of AMPs contributes greatly to the disruption of the bacterial cell wall, finally producing bactericidal ability.[22–27] In addition, AMPs enter into the bacteria and interact with the lipid bilayer to form a transmembrane pore, which can increase the susceptibility of the antimicrobial drug.[28] AMPs were also found to kill bacteria by inhibiting the intracellular functions, extracellular polymeric organisms, intracellular translocation, and inhibition of DNA/RNA/protein synthesis.[29,30] Due to the wide spectrum bactericidal ability, AMPs can even inhibit the formation of biofilms that are resistant to most antibiotics.[29,31] As one of the most promising alternatives to antibiotics, AMPs have shown promise to improve the outcome of medical devices with high risk of infections.

For the purpose of *in situ* anti-infection, surface modification of catheters or ureteral stents with AMPs represents a feasible and relatively safe strategy. The problem is that polymeric catheters or ureteral stents are relatively inert and hard to be stably modified with AMPs through traditional chemistry. In 2007, Lee *et al* developed a bio-inspired chemistry for surface modification based on the oxidative self-polymerization of dopamine (DPA).[32] The inspiration of dopamine for surface modification derived from the coexistence of catechol and amine in mussel foot proteins to form a synergistic interface adhesion.[33–36] The oxidation of dopamine results in a synergistic salt displacement of catechol and amine at the solid–liquid interface. The deposition of polydopamine (PDPA) can occur on almost all types of materials through catechol–metal coordination, electrostatic interaction, π–π interaction, hydrogen bonding and covalent reaction.[37–39] Since a further step conjugation can be easily achieved through amino- or thiol-mediated Michael addition, this mussel-inspired chemistry allows functionalization of biomolecules on a variety of biomaterials.[40–43] Recent studies also revealed that metal ion-assisted polydopamine adhesion can increase the coating stability and density, probably due to the metal–catechol-coordination-enhanced crosslinking network.[44] In this context, we consider to use metal–catechol-assisted mussel chemistry for AMP functionalization on commercially available catheters. Specifically, a typical AMP (RWRWRWC–NH_2)[45,46] with a thiol group in the residue of cysteine was introduced on a Cu^{2+}-coordinated polydopamine coating on PU ureteral stents (Scheme 1A). The stents with the AMP coating would *in situ* inhibit bacterial growth and biofilm formation, and finally reduce the deposition of struvite and hydroxyapatite crystals (Scheme 1B). In this work, we first optimized the bio-inspired coating and then evaluated its bactericidal and anti-crusting ability both *in vitro* and *in vivo*. We anticipate that this study would develop a safe, stable and effective antibacterial coating on urinary tract medical devices for long-term bacterial inhibition and encrustation prevention.

2. Materials and methods

2.1 Materials

Polyurethane (PU) ureteral stents were purchased from Jingxin Medical Supplies Company (Suzhou, China). The Spring laboratory pure water system based on RO-DI step-by-step purification technology was used to produce deionized water (dH_2O, 18.2 MΩ cm). Trypsin/EDTA (ethylenediaminetetraacetic acid) solution (0.25%), streptomycin, penicillin, RPMI (Roswell Park Memorial Institute) 1640 medium, MEM (minimum essential medium) and FBS (fetal bovine serum) were purchased from Gibco BRL (USA). Phosphate-buffered saline solution (PBS, 10 mmol L^{-1}, pH = 7.4) was purchased from HyClone (USA). Cell Counting Kit-8 (CCK-8) was purchased from Beyotime Biotechnology (Shanghai, China) and was used as received. Acridine Orange (AO) and propidium iodide (PI) were purchased from Shanghai Toscience Biotechnology (Shanghai, China) and were used as received. Dopamine hydrochloride (DPA·HCl) was obtained from HEOWNS, and creatinine (99%), urea (99%), ammonium chloride (NH_4Cl), sodium sulphate (Na_2SO_4), calcium chloride ($CaCl_2$), monobasic potassium phosphate (KH_2PO_4), sodium chloride (NaCl), potassium chloride (KCl), sodium oxalate ($C_2Na_2O_4$), trisodium citrate dihydrate ($C_6H_5Na_3O_7{\cdot}2H_2O$), magnesium chloride hexahydrate ($MgCl_2{\cdot}6H_2O$), copper sulfate pentahydrate ($CuSO_4{\cdot}5H_2O$) and tryptone were purchased from Hushi, Shanghai, China. Agar and yeast extract powder were purchased from Aladdin. LB liquid medium (1 L) containing 10 g sodium chloride, 5 g yeast extract, and 10 g tryptone and LB solid medium (1 L) containing

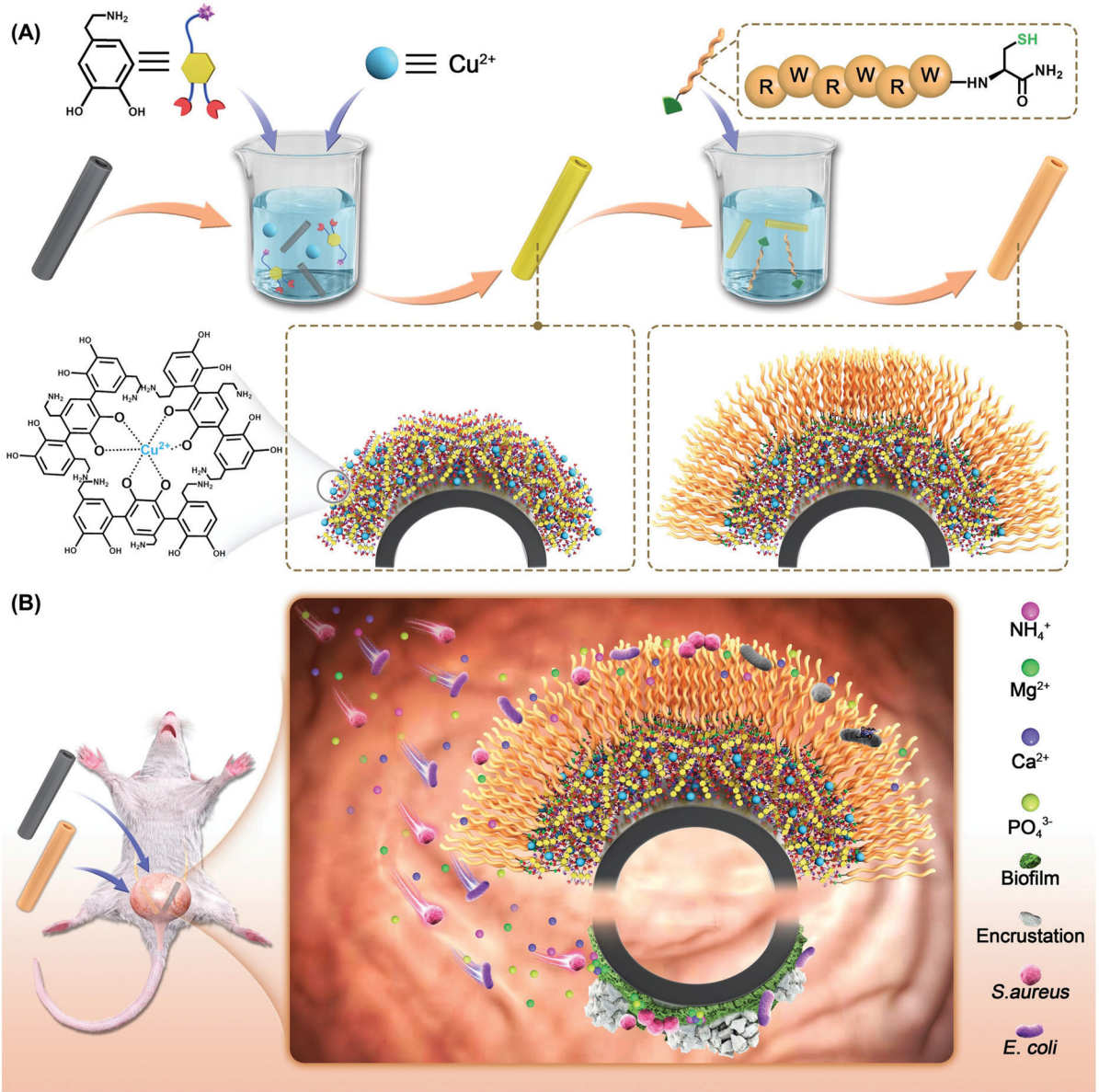

Scheme 1 Schematic illustration of the bio-inspired antibacterial and anti-encrustation strategy. (A) The molecular structures of DOPA and AMPs and the synthesis process of the bio-inspired antibacterial coating. (B) The bio-inspired antibacterial coating shows anti encrustation effect.

10 g sodium chloride, 5 g yeast extract, 10 g tryptone and 15 g aga. *E. coli* (ATCC 25922), *S. aureus* [CMCC(B) 26003] and *P. mirabilis* [CMCC(B)49005] were purchased from Shanghai Luwei Microbial Biotechnology (Shanghai, China). The brands and sources of all other biochemical reagents will be mentioned in the experimental methods as described below.

2.2 Preparation of a Cu-coordinated polydopamine AMP coating (PDPA@Cu–AMP)

(a) Pre-treatment of polystyrene (PS) 24-well plates. 24-Well plates were first treated with plasma (Fangrui Technology Shenzhen GD-5) to improve the wetting performance of the sample surface. The power was set at 180 W, and the treatment lasted for 300 s and repeated three times.

(b) Preparation of PDPA@Cu coatings. Five different ratios of DPA·HCl to Cu^{2+} (1000 : 0, 1000 : 25, 1000 : 75, 1000 : 125, and 1000 : 175) were used for deposition of PDPA@Cu coatings on the pre-treated 24-well plates. The PDPA@Cu coated wells were named PDPA@Cu-*X* (*X* = 0, 25, 75, 125, or 175). Typically, the plasma-treated 24-well plates were first added with 1 mL of pH 8.5 PBS and 0.1 mg of DPA·HCl, and then different volumes of $CuCl_2$ (1 mg mL^{-1}, 0 μL, 2.5 μL 7.5 μL, 12.5 μL and 17.5 μL) were added immediately. The reaction lasted at room temperature for 48 hours. The above solution was observed to appear brown after 2 min. After 48 h, the solution became dark brown with black solid precipitation. The PDPA@Cu-coated wells were then washed with deionized water 3 times, and dried with nitrogen. For coating on PU ureteral stents, the same procedures were applied.

(c) Preparation of PDPA@Cu-*X*–AMP coatings. The PDPA@Cu-coated wells were added with 0.1 mg of AMP (RWRWRWC–NH_2) and 1 mL of PBS (pH 8.5). After incubation at room temperature for 24 h, the wells were gently washed with 2 mL deionized water three times, and dried with nitrogen. Finally, different antibacterial coatings (named PDPA@Cu-*X*–AMP, X = 0, 25, 75, 125, or 175) were obtained.

For coating on SiO_2 slides, PU sheets or PU ureteral stents, the same procedures were applied according to the above three steps.

2.3 Characterization

Mass Spectrometry (MS) (Bruker solan X 70 FT-MS, Swiss) analysis was used to confirm the chemical structure of the AMP. X-ray photoelectron spectroscopy (XPS) (K-alpha, Thermo Fisher, USA), with a monochromatic Al Kα excitation source (1486.6 eV), was used to detect the surface elemental compositions of PDPA coatings and the elemental compositions of encrustations. Scanning electron microscopy (SEM) (ZEISS EVO 18) was used to characterize the surface morphology of the coating, the encrustation on stents, and the morphology of bacteria. An atomic force microscope (AFM) (Bruker Multimode 8) was used to characterize the roughness of the coating. A water contact angle meter (Dataphysics OCA20) was used to characterize the hydrophilicity of the surfaces.

2.4 *In vitro* antibacterial assays

(a) The effect of Cu^{2+} on the antibacterial ability of PDPA@Cu-*X*–AMP. Bacteria (*E. coli*) were cultured in LB liquid medium at 37 °C. The bacterial solution was taken out, and centrifuged, the supernatant was removed, and then *E. coli* was suspended with normal saline and diluted to an OD value of 0.1 (UV spectrophotometer at 625 nm). According to the absorbance and approximate bacterial concentration table given by Shanghai Luwei Microbial Biotechnology, when the OD value of *E. coli* solution at 625 nm is 0.1, the concentration is about 1.5×10^8 CFU mL^{-1}.

PDPA@Cu-*X* and PDPA@Cu-*X*–AMP (X = 0, 25, 75, 125, or 175) were coated on 24 well plates as described in Section 2.2. Bare 24 wells were selected as a control. Then the wells were disinfected with 75% alcohol for 5 mins, then were gently washed three times with 1 mL sterile normal saline and dried with nitrogen. *E. coli* (30 μL, concentration 1.5×10^5 CFU mL^{-1}) was dropped in each well, and the wells were covered with sterilized clingfilm seals for preserving moisture. The well plate was then put in a bacterial incubator at 37 °C for 24 h. After that, each well was added with 1 mL sterilized normal saline with sufficient mixing. 100 μL of the solution from each well was taken out and put into 9.9 mL sterile normal saline. 100 μL diluted solution was put into LB solid medium and incubated at 37 °C for 24 h.

(b) Broad-spectrum antibacterial effect of PDPA@Cu-75–AMP coatings. The coatings were grafted on to 10 mm double J stents and divided into three groups: control group, PDPA@Cu-75 coating and PDPA@Cu-75–AMP coating. Each group contained three wells. The sterilization method was the same as before. 30 μL *E. coli*, *S. aureus* and *P. mirabilis* (concentration 1.5×10^5 CFU mL^{-1}) were added into three wells of each group, respectively, and then the well plates were cultured and incubated according to the above method.

(c) Stability of PDPA@Cu-75–AMP coatings. The coating was grafted onto a 24-well plate and divided into two groups: control group and PDPA@Cu-75–AMP coating. Each group contained 10 wells. Each well was added into 1 mL sterile PBS (pH 8.5), and stored at 4 °C. One well of each group was taken out every week for a total of 10 weeks. The wells were taken out and sterilized by soaking in 0.5 mL 75% alcohol for 5 minutes. Then the wells were cleaned with 1.5 mL sterile PBS three times and dried with nitrogen. After that, *E. coli* (30 μL, concentration 1.5×10^5 CFU mL^{-1}) was dropped onto the surface of the control group and PDPA@Cu-75–AMP coating group according to the method above, and incubated at 37 °C for 24 h. After 24 h the well plates were taken out and diluted 1000 times with sterile normal saline. 100 μL of diluted solution was taken onto LB solid medium for 24 h.

(d) Bacterial inhibition of PDPA@Cu-75–AMP coatings on PU stents in artificial urine. In order to simulate the antibacterial effect of double J stents *in vivo*, an AMP was grafted onto 10 mm F8 (circumference 8 mm) stents and uncoated stents and PDPA@Cu-75 coating stents were added as a control. The stents were disinfected with 75% alcohol and placed into a sterile 24-well plate. One stent was put into one well and each well was put into 1 mL sterilized artificial urine (1 L contained 0.65 g $CaCl_2{\cdot}2H_2O$, 0.65 g $MgCl_2{\cdot}6H_2O$, 4.6 g NaCl, 2.3 g Na_2SO_4, 1.6 g KCl, 2.8 g KH_2PO_4, 1.0 g NH_4Cl, 20 mg sodium oxalate, 0.65 g sodium citrate·2 H_2O, 1.1 g creatinine and 25 g urea,[47] sterilized with a 0.45 μm pore size filter[17,48,49]). 10 μL *E. coli* (concentration 1.5×10^7 CFU mL^{-1}) was added to the artificial urine and cultured at 250 rpm and 37 °C. After 24 hours, half of the artificial urine was taken out and half of the fresh sterile artificial urine was added for further culture. After 1, 3, 7, and 14 days, the samples were taken out, rinsed with 2 mL sterile PBS 3 times and then placed in a 1 mL sterile normal saline centrifuge tube for 5 minutes in a 40 kHz ultrasonic bath. Then the solution was diluted 100 times, and 100 μL solution was taken for LB solid medium culture.

2.5 *In vitro* anti-encrustation

A total of 12 F8 stents with a length of 10 mm were selected, of which 4 were control group, 4 were PDPA@Cu-75 coating group, and the remaining 4 were PDPA@Cu-75–AMP coating group. They were weighed and placed in an *in vitro* bladder model; the model was composed of a 500 mL conical flask as a bladder *in vitro*; a rubber plug with three 5 mm holes can plug the taper bottle, two of the holes were put L type glass tube, one for artificial urine input port, the pipe orifice was 3 cm from the bottom, another tube for artificial urine output, and the orifice level was at 400 mL horizontal line. The thermometer was put in the last hole. Then a 0.5 mm diameter guide wire was used to suspend the stents in the *in vitro* bladder. One magnetic bead was taken into the conical flask. The *in vitro* bladder was placed flat on a constant temperature magnetic agitator at 37 °C and stirred at 60 rpm. Artificial urine containing 1×10^5 CFU mL^{-1}

P. mirabilis, which was stored in an ice water mixture to keep it fresh, was injected into the bladder at 0.5 mL min^{-1} with a peristaltic pump. In every 24 hours 10 mL artificial urine was removed from the bladder *in vitro* and measured with a pH meter (PHS-2F LEICI China). After 2 weeks, the stent was taken out, the loose crystallite was washed out with ultra-pure water, and then the stents were put into an oven to dry at 55 °C for 12 h. The stents were weighted after being dried. Two stents from each group were fixed with conductive adhesive and sputter-coated with gold for 20 min, and then were taken for SEM, and the other two for XPS measurements of crystal composition.

2.6 Cytotoxicity

(a) Live/dead cell staining. Due to the small surface area of the stents, it was difficult to have sufficient area for the cytotoxicity test (followed by standard ISO 10993-5:2009). The coating was grafted onto the wells of a 24-well plate, infected with 75% alcohol and dried with nitrogen. L929 cells were cultured in 1640 + 10%FPS medium. The wells in the plate were divided into three groups, which contained control, PDPA@Cu-75 coating and PDPA@Cu-75–AMP coating, with two wells in each group. The cell counting method was used to add 1 mL of 5×10^4 L929 cells to each well. After 24 h culture, the medium was sucked out, 1 mL fresh 1640 medium +15 μl AO + 10 μl PI was added, and the wells were incubated at 37 °C for 15 min in the dark. Then the medium was sucked out, and the wells were cleaned with 1 mL sterile PBS three times, and observed under a fluorescence microscope.

(b) CCK8 (Cell-Counting Kit 8) assay. Due to the small area of stents and the dark color of the PDPA coating, there will be a large error of OD value between the PDPA coating and the control group. The coating was grafted onto PU sheets. Therefore, 10 × 10 mm PU sheets were prepared and divided into 11 groups, which contained a control group, PDPA@Cu-*X* (*X* = 0, 25, 75, 125, and 175) group and PDPA@Cu-*X*–AMP, (*X* = 0, 25, 75, 125, and 175) group. Each PU sheet was sterile and washed with 2 mL PBS. PU sheets were then placed into sterile 24-well plates and added with 1 mL 1640 medium and 5×10^4 L929 cells for incubation in a 5% CO_2 cell incubator at 37 °C for 24 hours. Each sample was removed, and the surface was cleaned with 2 mL sterile PBS three times. The unattached cells were washed off, and then put PU sheets were taken into empty well plates. 300 μL EDTA was added to each well for 3 minutes, and 600 μL 1640 medium was added to terminate the digestion of the culture. The cells were washed off the PU sheet and then the cell suspension was centrifuged at 1000 rpm for 5 minutes. The supernatant was removed and the 600 μL 1640 medium was added. Each group of the cell suspension was divided into 6 parts on average, and every part was put into one well of the 96 well plate. 10 μL CCK8 solution was added into each well of the 96 well plate. The 96 well plates were incubated in the dark for 4 hours and measured with a microplate reader for OD value at 450 nm. The CCK8 assay was taken for the control group, PDPA@Cu-75 group and PDPA@Cu-75–AMP group for 48 and 72 h with the method mentioned above.

2.7 *In vivo* anti-encrustation

The animal experiments were approved by the Animal Ethics Committee of the First Affiliated Hospital of Soochow University for animal experiment (202103A211) and all experiments were performed in compliance with the authors' institute's policy on animal use and ethics. A total of 15 male Wistar/SD rats weighing 280–320 g were selected. It has been shown that rat urine is similar to human urine in terms of urine composition and crystallization behavior.[48,49] And most of the encrustation is formed at both ends of the stents, that is, the renal pelvis and bladder. Therefore, the rat bladder was used as an *in vivo* encrustation model. The PDPA@Cu-75 and PDPA@Cu-75–AMP group coatings were grafted onto 5 mm F4 PU ureteral stents. Unmodified ureteral stents were used as a negative control. Therefore, bare stents, PDPA@Cu-75 coating and PDPA@Cu-75–AMP coating stents were examined in *in vivo* experiments in a rat model (n = 5). The anesthetic solution (10% chloral hydrate, 0.3 mL/100 g live weight) was injected intraperitoneally for general anesthesia, and then stents (5 mm in length) were placed into the bladder of rats and stored for 14 days (Fig. 5A). After that, 1 mL of *P. mirabilis* (1.5×10^5 CFU mL^{-1}) was injected into bladders by the urethra at days 1, 4, 7 and 10. In 14 days, the rats were weighed and sacrificed. The abdomen was cut through a midline incision. The bladder was exposed and 100 μL of urine was extracted with a 1 mL sterile syringe. The urine in the bladder of the rats contained *P. mirabilis* that we injected before, so CLED agar plates were used for bacterial culture. The kidneys, ureter and bladder were removed completely. After macro assessment, bladder and kidney samples were preserved in 10% formalin solution (3.7% formaldehyde and 1.1% methanol) for 6 h, and then dehydrated with ethanol. After that, ethanol was cleared with xylene, and specimen was infiltrated with paraffin wax to support the tissue for thin sectioning. After the specimen was sliced and fixed on a glass slide, wax was removed by xylene and xylene substitutes. Then hematoxylin and eosin were used for hematoxylin–eosin staining (H&E), and after H&E staining, the specimen was histopathologically evaluated. After the stents were removed, cleaned and dried, SEM was used to observe the crusting of the stents.

2.8 Statistical analysis

The one way ANOVA test was used to evaluate the difference between sets of data in microbiology and animal experiments. Differences of statistical examinations were determined by the Tukey test. Microsoft Excel 2019 and IBM SPSS Statistics 22 were used to analyze statistics. The p value < 0.05 was considered as statistically significant.

3. Results and discussion

3.1 Preparation of PDPA@Cu–AMP coatings

To facilitate the conjugation of the AMP on the PDPA coating, here we employed a typical trivalent antibacterial dipeptide $(RW)_3$,[45,46] which was further capped with a cysteine at the C-terminal. The thiol group could be used to react with PDPA

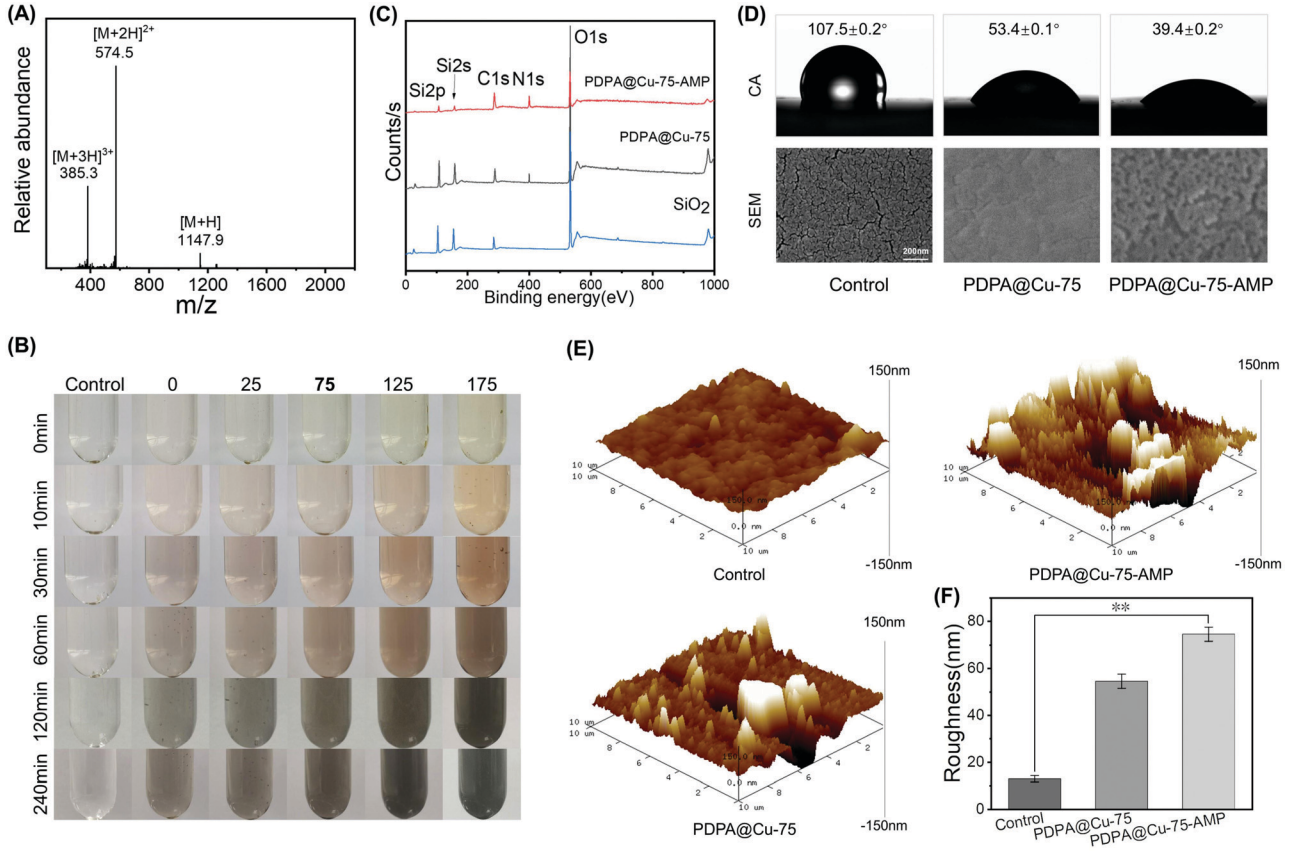

Fig. 1 (A) ESI mass spectrum of AMP(RW)$_3$. (B) The colours of PDPA with different Cu concentrations in different times. (C) XPS of bare SiO_2 slides, PDPA@Cu-75 coating and PDPA@Cu-75–AMP coating. (D) Contact angle and SEM of bare PU sheets, PDPA@Cu-75 coating and PDPA@Cu-75–AMP coating on PU sheets. (E) AFM and (F) roughness of bare PU sheets, PDPA@Cu-75 coating and PDPA@Cu-75–AMP coating on PU sheets. The error bars represent SD. Statistically significant differences are indicated by $*p < 0.05$ or $**p < 0.005$ compared with the control group.

through Michael addition. Electrospray ionization mass spectrometry (ESI-MS) analysis was used to confirm the success of peptide molecular synthesis. As shown in Fig. 1A, the monoisotopic mass $[M + H]^+$ of AMP (RWRWRWC–NH_2) was found at 1147.9 Da, which was in line with its theoretical molecular weight (1147.39 Da), according to the chemical structure. The preparation of the PDPA@Cu-75–AMP coating was divided into two steps. The first step was to self-polymerize DPA into PDPA under an alkaline condition. SiO_2 slides, PU sheets or stents were used to deposit polydopamine on the surface. In this work, we considered to employ Cu^{2+} for an improved PDPA coating. This is due to the strong coordination between Cu^{2+} and the catechol of DPA, which would enhance the coating density and stability. As shown in Fig. 1B, the self-polymerization of DPA and the resultant PDPA coating thickness were highly dependent on the Cu^{2+} concentration. At the same reaction time, the higher the Cu^{2+} concentration, the darker the colour of the solution observed, while with the same Cu^{2+} concentration, a longer reaction time led to darker colour of the solution. This result indicated the importance of the reaction time and Cu^{2+} content during DPA self-polymerization, which would determine the grafting thickness and stability of a PDPA@Cu-*X* coating. Thus, an optimization of the Cu-assisted DPA polymerization is needed.

When the first step PDPA coating was completed, the quinone bonds formed during the self-polymerization process were exposed to the surface of the coating. Upon the addition of the cysteine-capped AMP (even at room temperature), it could be grafted onto the PDPA surface to form an antibacterial coating through quinone–thiol Michael addition reaction. In order to verify that the PDPA@Cu coating and AMP could be steadily grafted onto the surface of the above materials (*e.g.*, SiO_2 slides, PU substrate or stents), we then chose a typical Cu-coordinated PDPA coating (PDPA@Cu) for AMP conjugation (PDPA@Cu–AMP). Then, XPS analysis of the untreated (control), PDPA@Cu and PDPA@Cu–AMP was performed to examine the surface chemical compositions. As shown in Fig. 1C, the N 1s signal (399.8 eV) from the surfaces of PDPA@Cu and PDPA@Cu–AMP was obviously observed, while the Si 2p and Si 2s signals from SiO_2 were also shielded. In contrast, the control group showed no N 1s signal. Furthermore, due to catechol–metal coordination, the XPS spectrum also showed a peak of Cu 2p signal (will be discussed in the next section). Quantitative analysis of PDPA@Cu revealed that the contents of C, N and Cu elements were 91.84%, 7.21% and 0.95%, respectively. The next step reaction with the AMP also led to an increase of the N content (22.7%), and the C/N ratio was calculated to be 77 : 23, which was between that of a pure PDPA

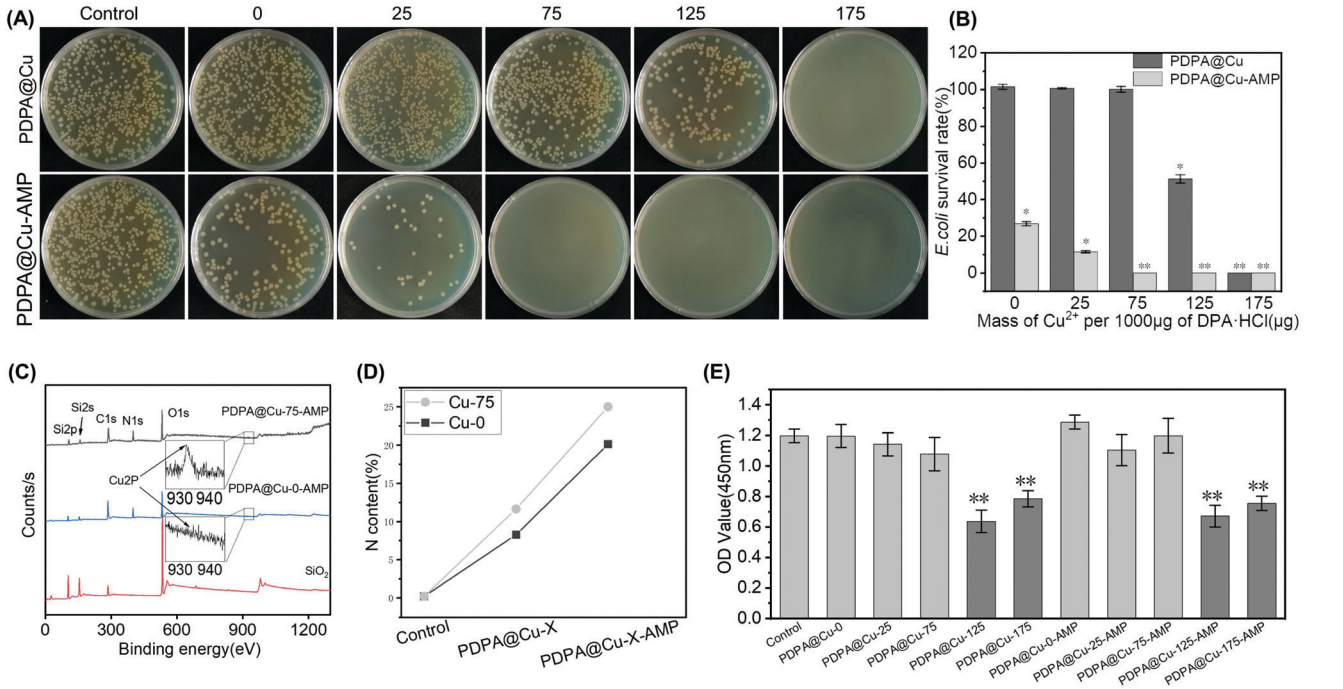

Fig. 2 (A) Bacterial growth on LB solid medium and (B) *E. coli* survival rate after contact with the control group, PDPA@Cu with different mass ratios of DPA to Cu^{2+} group and PDPA@Cu–AMP coating with different mass ratios of DPA to Cu^{2+} group for 24 h. (C) XPS of SiO_2 slides, PDPA@Cu-0–AMP and PDPA@Cu-75–AMP coatings. (D) Different N contents of control, PDPA@Cu-0/75, and PDPA@Cu-0/75–AMP coatings. (E) CCK8 assay of control, different rate of DPA to Cu^{2+} PDPA@Cu and PDPA@Cu–AMP coating groups. The error bars represent SD, and statistically significant differences are indicated by $*p < 0.05$ or $**p < 0.005$ compared with the control group.

coating (90 : 10) and that of the AMP (73 : 27), implying the success of peptide conjugation.

The surface wettability of different surfaces was also characterized with a water contact angle meter. As shown in Fig. 1D, the PDPA@Cu coating could significantly increase the surface hydrophilicity, which was in line with previous studies.[45,50,51] For example, the contact angle of a bare PU sheet was 107.5 ± 0.2°. After PDPA@Cu coating, the surface contact angle was significantly reduced to 53.4 ± 0.1°. In addition, a next step AMP conjugation further resulted in the decrease of contact angle (39.4 ± 0.2°), probably due to the high hydrophilicity of trivalent RW sequences. SEM and AFM were also used to study the surface morphology of substrates with different treatments (Fig. 1E). SEM showed that the surfaces with coatings were significantly different from a bare PU surface (Fig. 1D). It was also found that PDPA@Cu and PDPA@Cu–APM coatings showed a rougher surface than the bare PU substrate. Quantitative analysis of the AFM images confirmed the increased surface roughness of PU substrates with coatings (Fig. 1F), further confirming the success of PDPA coating. Taken together, these results jointly demonstrated that the Cu^{2+}-assisted DPA polymerization could be efficiently used for surface modification of PU-based materials, indicating the potential for antibacterial functionalization of commercially available PU catheters.

3.2 Optimization of the PDPA@Cu–AMP coatings

In this work, Cu^{2+} was used to accelerate DPA self-polymerization, in order to increase the thickness of the coating, the density of AMP graft sites, and also the stability of the whole layer. Although Cu^{2+} possesses inherent bactericidal activity, it will also elicit significant cytotoxicity when the concentration reaches a relatively high value. Thus, it is necessary to select an appropriate Cu^{2+} concentration capable of not only improving the antibacterial performance of the PDPA coating but also exhibiting low or no cytotoxicity. To this end, five groups of PDAP@Cu and PDAP@Cu–AMP coatings on PU substrates with different Cu^{2+} to DPA ratios were prepared, and their biocompatibility and antibacterial activity were comprehensively studied. *E. coli* was used as the bacteria model for antibacterial assays. As shown in Fig. 2A, the PDPA coating without Cu coordination had no significant antibacterial effect. When Cu^{2+} was cooperated into PDPA, the *E. coli* colony was gradually decreased on the LB solid plate. When the Cu^{2+}/DPA ratio increased to 175 : 1000, no *E. coli* could be observed on the plate, indicating a Cu^{2+}-derived antibacterial activity of the PDPA@Cu-175 coating. Quantitative analysis further revealed that the PDPA@Cu-25 and PDPA@Cu-75 coatings had no significant antibacterial ability (Fig. 2B), implying the negligible influence of Cu^{2+} on bacterial survival when the Cu^{2+}/DPA ratio was lower than 75 : 1000.

The AMP-conjugated coatings were also applied for antibacterial assays. We could find that the number of bacterial colonies was significantly reduced on the PDPA@Cu-0–AMP coating compared with the control group (PDPA@Cu-0). Unfortunately, there was still considerable bacterial growth observed. This result indicated that although the AMP molecules were

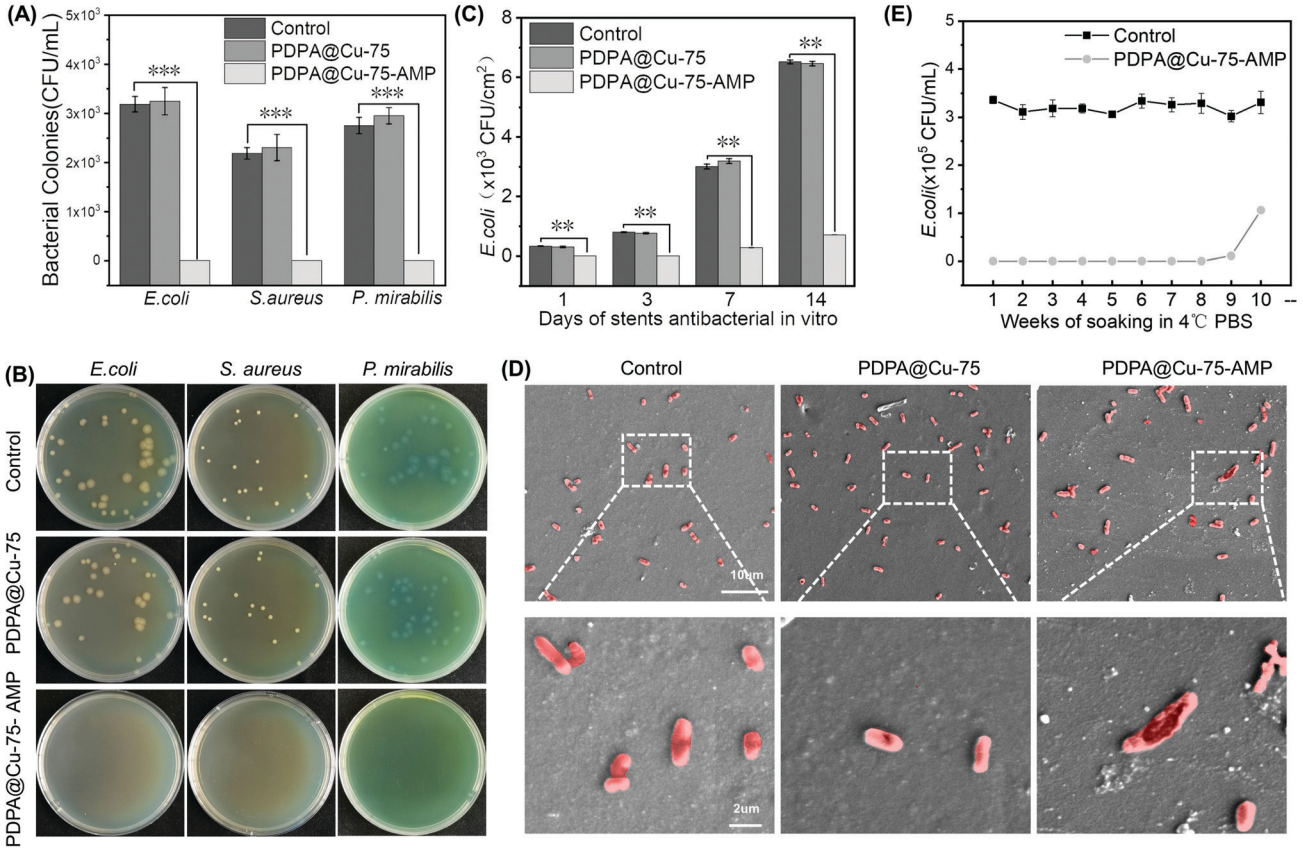

Fig. 3 (A) and (B) antibacterial effect of bare stents (control), PDPA@Cu-75 and PDPA@Cu-75–AMP coatings against *E. coli*, *S. aureus* and *P. mirabilis*. (C) Comparison of bare stents (control), PDPA@Cu-75 and PDPA@Cu-75–AMP coating DJ stents in 2 weeks of continuous *in vitro* antibacterial experiment. (D) SEM of *E. coli* after stay on bare PU sheets, PDPA@Cu-75 and PDPA@Cu-75–AMP coating PU sheets for 24 hours. (E) Time of decomposition failure of the PDPA@Cu-75–AMP coating after soaking in PBS at 4 °C. The error bars represent SD. Statistically significant differences are indicated by $^{**}p < 0.005$ or $^{***}p < 0.001$ compared with the control group.

grafted on the PU surface, the AMP grafting density was not enough to show a desirable antibacterial effect. In contrast, Cu^{2+} coordinated PDPA coatings all showed higher antibacterial activity compared to that of PDPA@Cu-0–AMP. As shown in Fig. 2A, there were only a few *E. coli* colonies on the surface of the PDPA@Cu-25–AMP coating, and no bacteria existed on the other groups with higher concentration of Cu coordination (*i.e.*, the PDPA@Cu-75–AMP, PDPA@Cu-125–AMP and PDPA@Cu-175–AMP coatings). Quantitative analysis of the *E. coli* survival rate indicated that the groups introduced with higher concentrations of Cu^{2+} could thoroughly eliminate surface bacteria (Fig. 2B), implying that the AMP densities on a Cu^{2+}-coordinated PDPA coating were significantly increased, and it could bring potent bacterial killing ability compared with the Cu^{2+} free control group (PDPA@Cu-0–AMP). These results verified our hypothesis that Cu^{2+} could enhance the self-polymerization of DPA and subsequently improve the AMP grafting efficiency.

We further analyzed the surface Cu elements using XPS. Fig. 2C showed that the Cu 2P peak (932.4 eV) was obvious in the spectrum of the PDPA@Cu-75–AMP coating, but not in the PDPA@Cu-0–AMP coating. Moreover, the N content of PDPA@Cu-75–AMP was significantly higher than that of PDPA@Cu-0–AMP (Fig. 2D), suggesting that Cu^{2+} participation in the self-polymerization of DPA could increase the grafting amount of the PDPA coating, and this then improved the AMP grafting density and subsequently enhanced the surface antibacterial properties. Since we have figured out the lowest Cu^{2+} concentration for an effective AMP conjugation, the Cu^{2+}-derived cytotoxicity was further evaluated by a CCK8 assay. CCK8 assay is based on an electron carrier 1-methoxy 5-methylphenazine dimethyl sulfate (1-methoxy PMS), which could be reduced to a highly water-soluble yellow haze (formazan) by dehydrogenase in the cell mitochondria. The amount of haze generated was proportional to the number of living cells. Enzyme linked immunoassay (ELISA) was used to measure the light absorption value at 450 nm, which could indirectly reflect the number of living cells. The results of CCK8 assay showed that, at lower Cu^{2+} concentrations (*e.g.*, PDPA@Cu-0–AMP, PDPA@Cu-25–AMP, and PDPA@Cu-75–AMP), no significant cytotoxicity was observed. In contrast, the high Cu coatings including PDPA@Cu-125, PDPA@Cu-175–AMP, PDPA@Cu-125–AMP, and PDPA@Cu-175–AMP showed an obvious inhibition of cell proliferation (L929 cells) (Fig. 2E). The results indicated that a potentially safe PDPA@Cu coating for *in vivo* use should be prepared using the Cu^{2+}/DPA

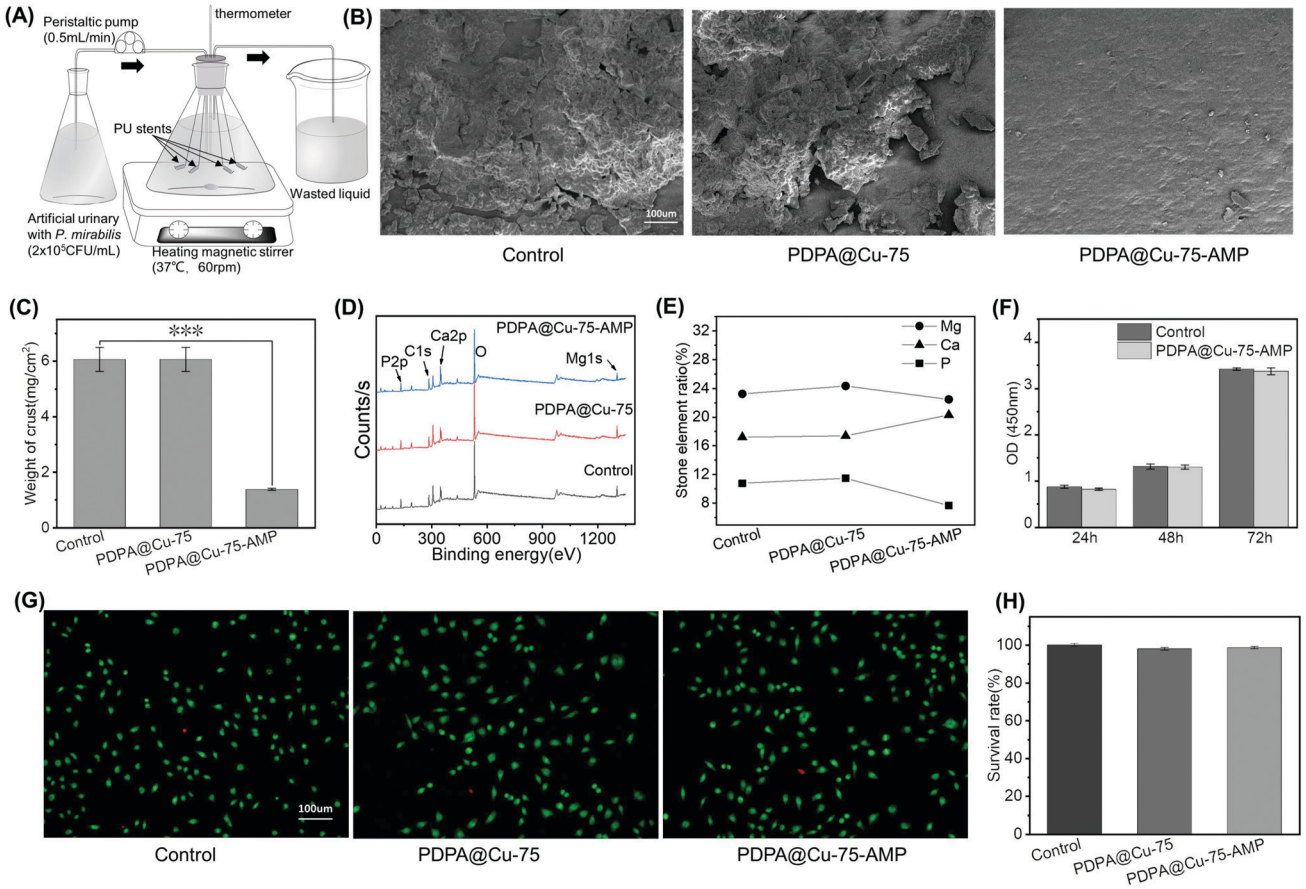

Fig. 4 (A) Schematic of the *in vitro* bladder model. (B) SEM of bare stents, PDPA@Cu-75 and PDPA@Cu-75–AMP coating surfaces after 2 weeks of encrustation experiment *in vitro*. (C) Mass of crystal deposit on bare stents, PDPA@Cu-75 and PDPA@Cu-75–AMP coating surfaces after 2 weeks of encrustation experiment *in vitro*. (D) XPS of crystal deposit and (E) changes in the proportion of P, Ca, and Mg in bare stents, PDPA@Cu-75 and PDPA@Cu-75–AMP coating stents. (F) 24, 48, and 72 h of CCK8 assay of control and PDPA@Cu–AMP group. (G) Living and dead cell staining and (H) the survival rate of L929 cells after being cultured on bare PU sheets, PDPA@Cu-75 and PDPA@Cu-75–AMP coating PU sheets for 24 h. The error bars represent SD. Statistically significant differences are indicated by ***$p < 0.001$ compared with the control group.

ratio lower than 75 : 1000.[52] Since the PDPA@Cu-0–AMP and PDPA@Cu-25–AMP coatings both exhibited relatively lower antibacterial activity, in our following experiments, the PDPA@Cu-75–AMP was used as the optimal coating, because of its double advantages in biocompatibility and antibacterial ability.

3.3 Antimicrobial activity of the PDPA@Cu-75–AMP coating *in vitro*

The AMP $(RW)_3$ used in this study possesses a broad spectrum of antibacterial properties. It has been revealed that the main pathogenic bacteria in urinary system infections are Gram-negative bacteria such as *E. coli* and *P. mirabilis* and Gram-positive *S. aureus*. Since the ultimate application of our coating is for surface modification of ureteral stents or ureter catheters, *E. coli*, *P. mirabilis* and *S. aureus* thus were all chosen to test the *in vitro* antibacterial activity of our coating. The PDPA@Cu-75–AMP coating was first prepared onto F8 ureteral stents, and then their bacterial inhibition (24 h) was tested against the three Gram-positive and Gram-negative bacteria. Compared with the bare and the AMP free PDPA@Cu-75 coated stents, the PDPA@Cu-75–AMP coated stents could significantly inhibit all kinds of bacterial growth (including *E. coli*, *P. mirabilis* and *S. aureus*) on the surface (Fig. 3A and B), indicating the broad spectrum of antibacterial activity. In addition, the long-term antibacterial effect of the PDPA@Cu-75–AMP coating was further tested. Our results showed that the PDPA@Cu-75–AMP coating on ureteral stents could continuously inhibit bacterial growth for two weeks (Fig. 3C). In contrast, bacteria on the bare and AMP free PDPA@Cu-75 surface showed rapid proliferation in one week. Although the antibacterial efficiency of the PDPA@Cu-75–AMP coating showed a slight decrease, it still had significantly better antibacterial activity compared to the others. The results demonstrated that our PDPA@Cu-75–AMP coating could not only immediately kill the surface bound bacteria but also enable long-term bacterial inhibition.

The morphology and membrane integrity of the surface bound bacteria (*E. coli*) were characterized by SEM. On the surfaces of the control group and the PDPA@Cu-75 coating group, bacteria could maintain the integrity of the cell wall (Fig. 3D). On the contrary, the bacteria on PDPA@Cu-75–AMP coated surfaces showed an incomplete cell membrane,

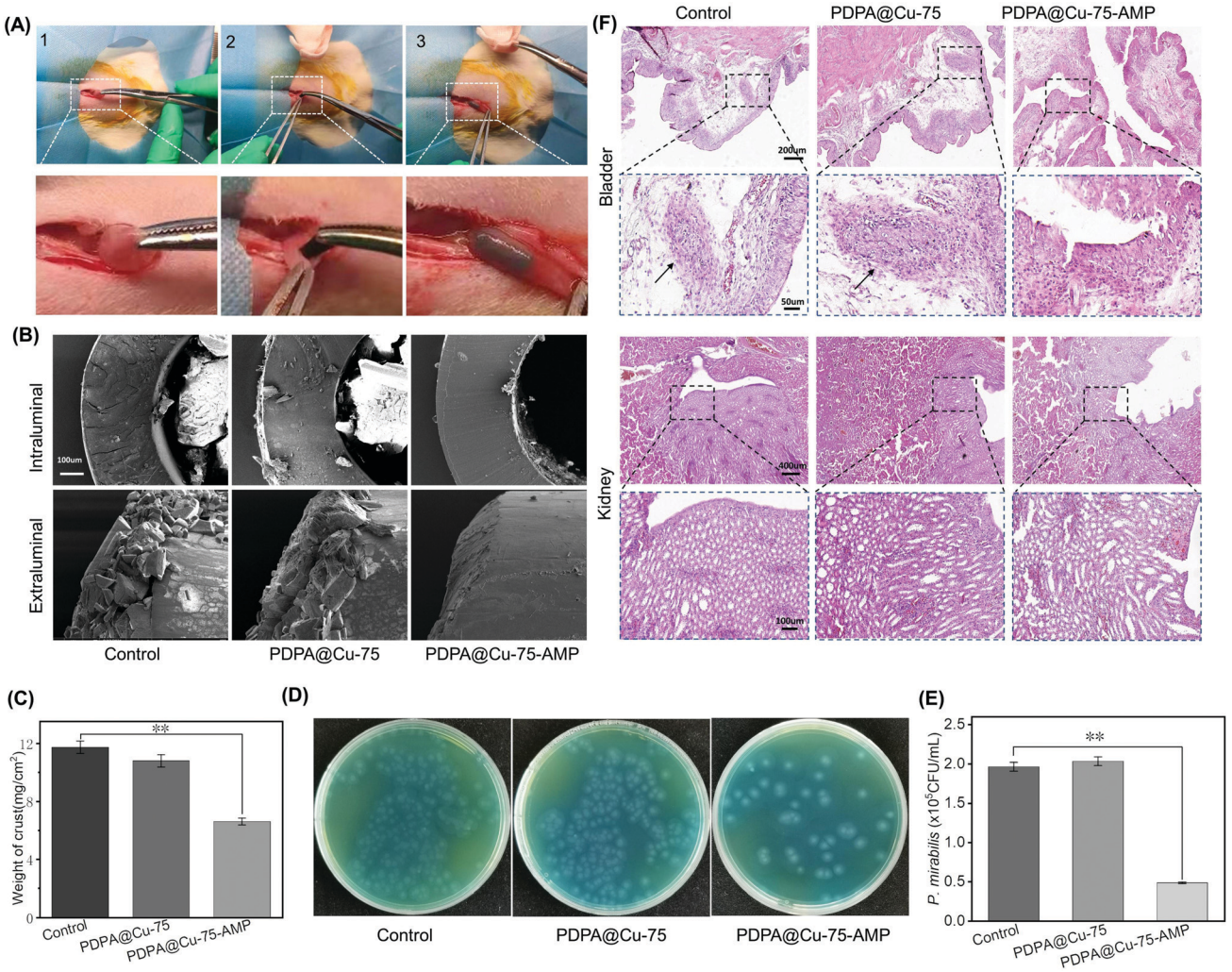

Fig. 5 (A) 1 Rat bladder, 2 the stent entered the bladder from the bottom and 3 stent in the bladder. (B) SEM of rats' intravesical stents lumen and surface and (C) the mass of deposit in control, PDPA@Cu-75 and PDPA@Cu-75–AMP coating groups. (D) Bare stent, PDPA@Cu-75 and PDPA@Cu-75–AMP coating stent group of rats' urines cultured in CLED agar plate medium and (E) the colony counting of *P. mirabilis*. (F) H&E staining of pathological sections of bladder and kidneys of rats in control, PDPA@Cu-75 and PDPA@Cu-75–AMP coating groups; the arrow indicates neutrophil infiltration. The error bars represent SD. Statistically significant differences are indicated by $^{**}p < 0.005$ compared with the control group.

indicating that surface conjugated antibacterial peptides could efficiently kill the bacteria contacted. The result demonstrated that the conjugated AMP on PU ureteral stents did not lose its antibacterial activity. Further in this study, ten groups of PDPA@Cu-75–AMP coatings were soaked in PBS. The antibacterial activity for each group at different weeks was tested. It was found that the PDPA@Cu-75–AMP coating could maintain excellent antibacterial properties until the 9th week (Fig. 3E), indicating the long-term stability of the AMP and the PDPA coating. This result suggested that the PDPA@Cu-75–AMP coating is very suitable for indwelling stents in the urinary system, which are always implanted in the bladder for months.

3.4 Anti-encrustation of the PDPA@Cu-75–AMP coating *in vitro*

The formation of encrustation on the ureteral stent surface can lead to increased infection, obstruction, and also the difficulty to remove stents. The reason for encrustation formation is mainly due to bacterial infection and biofilm formation, especially *P. mirabilis*, which can decompose urea, increase urine pH, and result in a microenvironment that is inclined to form a crust on ureteral stent surfaces. Since our PDPA@Cu-75–AMP-coating possesses broad-spectrum antibacterial and anti-biofilm properties, we designed an *in vitro* bladder model (Fig. 4A) to simulate the crusting process of ureteral stents, and evaluated the effect of our coating on encrustation prevention.

After 2 weeks of incubation in artificial urine with *P. mirabilis*, the thermometers, magnetic beads, glass tubes, and conical bottles were covered with a layer of white crusts; moreover, the artificial urine was turbid. The pH of artificial urine also increased from less than 5.5 to 8.5 in two weeks, and balanced to a value between 8.3 and 8.5 in the later period. The phenomenon implied the decomposition of urea by *P. mirabilis*,

and the increased pH value would provide a favourable condition for the deposition of Mg^{2+} and Ca^{2+}. On the surfaces of bare and the PDPA@Cu-75-coated stents, there were not only relatively firm attachments, but also loose stones. The stents were placed into ultra-pure water to wash away the loose stones, and then dried with nitrogen. The weight of the crust on each stent was obtained. SEM images of the stent surfaces showed that the amount of crust of the PDPA@Cu-75–AMP-coated stents was significantly less compared with that on the control and the PDPA@Cu-75-coated ones (Fig. 4B). We can clearly observe that the groups of control and the PDPA@Cu-75 were covered with a mass of encrustation, and the real surface of the polymer stents could hardly be observed. In contrast, the PDPA@Cu-75–AMP stent showed a clean surface, and only sporadic and small encrustation could be found. The average crusting weight in the control and the PDPA@Cu-75 group showed no statistical significance, while there was statistical significance for the group of PDPA@Cu-75–AMP (Fig. 4C). The crust on the PDPA@Cu-75–AMP surface was only 23% of the other two groups. Since the components of these stones contain mainly magnesium ammonium phosphate encrustation (struvite) produced by urease-producing bacteria, the contents of Ca, Mg and P in these stones were then semi-quantitatively characterized by XPS (Fig. 4D and E). XPS analysis showed that there was no significant difference in the components of these stones in control, PDPA@Cu-75, and PDPA@Cu-75–AMP groups. We found that these stones were mainly struvite. Moreover, the contents of P and Mg in the PDPA@Cu-75–AMP group were significantly less than those of the other two groups (Fig. 4F). The result implied that the PDPA@Cu-75–AMP coating had a long-term (2 week) and efficient inhibitory effect on encrustation formation induced by urease-producing bacteria, and this property is highly desired for indwelling catheters or stents.

3.5 Cytotoxicity of the PDPA@Cu-75–AMP coating

We have verified that the PDPA@Cu-75–AMP coating showed the best antibacterial and anti-encrustation performance. We then further investigated the biocompatibility of this coating prior to applying *in vivo* studies on its ability to inhibit bacteria and prevent encrustation. CCK8 and live/death staining experiments were performed to evaluate the cytotoxicity of the PDPA@Cu-75–AMP coating. CCK8 assay was performed on L929 cells after 24, 48 and72 hours of culture on the PDPA@Cu-75-AMP and the control surfaces. It was found that there was no significant difference in cell proliferation between the two groups in 3 days (Fig. 4F), suggesting the negligible influence of the AMP- and Cu^{2+}-containing coating on cell growth.

Live/Dead staining was further applied to provide an intuitive cytotoxicity of the coating. Live/Dead staining is a very efficient tool to analyze the viability and adherence of cells on surfaces. The assay is based on two fluorescent dyes green AO and red PI. AO has membrane permeability and can penetrate the live cell membrane to stain nuclear DNA and RNA. PI is a DNA-binding dye with excitation and emission wavelengths of 488 nm and 630 nm, respectively. It produces red fluorescence, but has no membrane permeability, and cannot pass through living cell membranes, thus enabling the staining of only dead cells. After culture on the PDPA@Cu-75–AMP and the control surfaces for 24 h, L929 cells were stained with AO and PI. According to the staining mechanism, normal cells could be coloured with green, early apoptotic cells showed weak red fluorescence, late apoptotic cells showed enhanced red, and necrotic cells showed strong red fluorescence. It was observed that cells adhered well on the surfaces, and almost all the cells were green stained (Fig. 4G). Cell counting showed that the number of dead cells is very small, less than 1% (Fig. 4H). Moreover, the PDPA@Cu-75–AMP group showed no significant difference as compared to the bare (control) group. The result indicated that the mussel-inspired, Cu-coordinated and APM-modified coating had negligible cytotoxicity.

3.6 *In vivo* anti-encrustation of the PDPA@Cu-75–AMP coating

With this biocompatible, antibacterial and anti-encrustation coating in hand, we then applied it on commercially available PU stents to investigate the *in vivo* properties. In this study, Wistar/SD rats were used for *in vivo* tests because their urine and encrustation are similar to those of humans. Stents with or without the PDPA@Cu-75–AMP coating were surgically inserted into the bladder of rats followed by injection of *P. mirabilis* into the bladders (Fig. 5A). After 2 weeks, all the stents were removed from the bladder, and cleaned with ultrapure water. SEM was first used to check the surface crusting morphology after drying with nitrogen. As rats are living creatures, and the bladder can contract involuntarily and produce friction between the stent surface and the bladder, it is difficult to form more stones on the stent surface as the surfaces in the *in vitro* bladder model. Nevertheless, the stent orifice and lumen are difficult to rub and touch, which is conducive to the formation of stone in a bacteria-containing environment. SEM images showed that, in the control and the PDPA@Cu-75 group, there was plenty of encrustation in both the orifice and the lumen. Moreover, the encrustation had already blocked the stents (Fig. 5B). In contrast, in the PDPA@Cu-75–AMP group, only a few calculi formed in the orifice and the lumen, and the lumen was still unimpeded. The encrustation was then carefully removed and quantitatively analyzed. As shown in Fig. 5C, the weight of stones in the PDPA@Cu-75–AMP group was significantly reduced compared with the control and PDPA@Cu-75 group (Fig. 5C). This result was in line with that of the *in vitro* bladder model, in which the PDPA@Cu-75–AMP coating showed superior anti-crusting abilities because of the antibacterial activity of AMP.

To confirm the *in vivo* antibacterial ability of our coating, urine from the bladders of rats was also taken out for bacterial culture (Fig. 5D). It was found that bacteria on the PDPA@Cu-75–AMP coating, PDPA@Cu-75 and control groups were mainly *P. mirabilis*. As expected, the bacterial colony in the group of PDPA@Cu-75–AMP was significantly reduced compared with control groups (Fig. 5E), indicating the efficient antibacterial

ability *in vivo*. The result also verified that the anti-encrustation of PDPA@Cu-75–AMP was directly related to the antibacterial ability. Although the PDPA@Cu-75–AMP coating could not completely kill bacteria in urine, it could still effectively inhibit bacterial reproduction, inhibit the development of UTIs and reduce the degree of infection.

Further in animal experiments, the bladders and kidneys from all groups of rats were examined with H&E staining (Fig. 5F). It was found that the bladder tissues in the control and PDPA@Cu-75 coating groups showed inflammation. H&E images of the control and PDPA@Cu-75 groups both had obvious infiltration of neutrophils, while in the PDPA@Cu-75–AMP group, infiltration of neutrophils in bladder tissues was significantly reduced. Moreover, no obvious abnormality was found in the renal pathological sections of all three groups. This may be because the anti-reflux function of the ureter was not damaged, and the infected urine could not retrograde into the kidney. We also inferred that the inflammatory inhibition of the PDPA@Cu-75–AMP group was due to the antibacterial ability, which reduced the intrusion of bacteria into bladder tissues and also the whole urinary system.

4. Conclusions

In summary, here we reported a Cu^{2+}-assisted mussel-inspired strategy for surface antibacterial modification of catheters with AMP. We optimized the bio-inspired coating and then evaluated its bactericidal and anti-crusting ability. The results confirmed that Cu^{2+}-coordinated antibacterial coating showed improved stability, antibacterial effect, and good biocompatibility both *in vitro* and *in vivo*. More importantly, the mussel-inspired, Cu^{2+}-coordinated, AMP-modified stents could *in situ* inhibit bacterial growth and biofilm formation, showing long-term anti-infection and encrustation prevention *in vivo*. The developed bioinspired strategy in this work may show promise for fabrication of efficient antibacterial surfaces on urinary tract medical devices with long-term bacterial inhibitory effects and encrustation prevention ability.

Author contributions

Qin Yao: methodology, investigation, data curation and writing original draft. Binghai Chen: conceptualization, methodology, investigation, data curation, and writing original draft. Jiaxiang Bai: conceptualization, resources, and supervision. Wenbo He: formal analysis and visualization. Xu Chen: visualization and investigation. Dechun Geng: conceptualization, resources, and supervision. Guoqing Pan: conceptualization, resources, supervision, writing, review & editing and project administration.

Conflicts of interest

There are no conflicts to declare.

Acknowledgements

We greatly acknowledge the financial support from the National Key Research and Development Program of China (2019YFA0112000), the National Natural Science Foundation of China (21875092 and 82072425), the Natural Science Foundation of Jiangsu Province (BK20211123), the Social Development Foundation of Zhenjiang (SH2021033), the Innovation and Entrepreneurship Program of Jiangsu Province, and the ''Six Talent Peaks'' program of Jiangsu Province (2018-XCL-013), and the Special Project of Diagnosis and Treatment for Clinical Diseases of Suzhou (LCZX202003).

Notes and references

1 F. Gong, X. Cheng, S. Wang, Y. Zhao, Y. Gao and H. Cai, *Acta Biomater.*, 2010, **6**, 534–546.
2 J. Zhao, Z. Cao, H. Lin, H. Yang, J. Li, X. Li, B. Zhang and K. Yang, *J. Mater. Sci.: Mater. Med.*, 2019, **30**, 83.
3 P. Singha, J. Locklin and H. Handa, *Acta Biomater.*, 2017, **50**, 20–40.
4 A. Mosayyebi, C. Manes, D. Carugo and B. K. Somani, *Curr. Urol. Rep.*, 2018, **19**, 35.
5 B. Saltzman, *Urol. Clin. North Am.*, 1988, **15**, 481–491.
6 D. J. Stickler, *J. Intern. Med.*, 2014, **276**, 120–129.
7 I. Scarneciu, S. Lupu, C. Pricop and C. Scarneciu, *Pak. J. Med. Sci.*, 2015, **31**, 522–526.
8 G. Giannarini, F. X. Keeley, Jr., F. Valent, F. Manassero, A. Mogorovich, R. Autorino and C. Selli, *BJU Int.*, 2011, **107**, 648–654.
9 I. Singh, N. P. Gupta, A. K. Hemal, M. Aron, A. Seth and P. N. Dogra, *Urology*, 2001, **58**, 526–531.
10 C. V. Gould, C. A. Umscheid, R. K. Agarwal, G. Kuntz, D. A. Pegues and C. Healthcare Infection Control Practices Advisory, *Infect. Control Hosp. Epidemiol.*, 2010, **31**, 319–326.
11 D. G. Maki and P. A. Tambyah, *Emerging Infect. Dis.*, 2001, **7**, 342–347.
12 J. W. Warren, L. Steinberg, J. R. Hebel and J. H. Tenney, *Arch. Intern. Med.*, 1989, **149**, 1535–1537.
13 M. Wang and T. Tang, *J. Orthop. Translat.*, 2019, **17**, 42–54.
14 S. M. Jacobsen, D. J. Stickler, H. L. Mobley and M. E. Shirtliff, *Clin. Microbiol. Rev.*, 2008, **21**, 26–59.
15 M. Ramstedt, I. A. C. Ribeiro, H. Bujdakova, F. J. M. Mergulhao, L. Jordao, P. Thomsen, M. Alm, M. Burmolle, T. Vladkova, F. Can, M. Reches, M. Riool, A. Barros, R. L. Reis, E. Meaurio, J. Kikhney, A. Moter, S. A. J. Zaat and J. Sjollema, *Macromol. Biosci.*, 2019, **19**, e1800384.
16 R. Wasfi, S. M. Hamed, M. A. Amer and L. I. Fahmy, *Front. Cell. Infect. Microbiol.*, 2020, **10**, 414.
17 K. Belfield, X. Chen, E. F. Smith, W. Ashraf and R. Bayston, *Acta Biomater.*, 2019, **90**, 157–168.
18 B. D. Jones and H. L. Mobley, *Infect. Immun.*, 1987, **55**, 2198–2203.
19 V. Zumstein, P. Betschart, W. C. Albrich, M. T. Buhmann, Q. Ren, H. P. Schmid and D. Abt, *Swiss Med. Wkly.*, 2017, **147**, w14408.

20 A. Torzewska and A. Rozalski, *Microbiol. Res.*, 2014, **169**, 579–584.
21 J. M. Ageitos, A. Sánchez-Pérez, P. Calo-Mata and T. G. Villa, *Biochem. Pharmacol.*, 2017, **133**, 117–138.
22 C. Monteiro, F. Costa, A. M. Pirttila, M. V. Tejesvi and M. C. L. Martins, *Sci. Rep.*, 2019, **9**, 10753.
23 M. Zasloff, *Nature*, 2002, **415**, 389–395.
24 S. A. Baltzer and M. H. Brown, *J. Mol. Microbiol. Biotechnol.*, 2011, **20**, 228–235.
25 J. Fernebro, *Drug Resist. Updates*, 2011, **14**, 125–139.
26 G. Laverty, S. P. Gorman and B. F. Gilmore, *Int. J. Mol. Sci.*, 2011, **12**, 6566–6596.
27 M. D. Seo, H. S. Won, J. H. Kim, T. Mishig-Ochir and B. J. Lee, *Molecules*, 2012, **17**, 12276–12286.
28 K. A. Brogden, *Nat. Rev. Microbiol.*, 2005, **3**, 238–250.
29 A. C. Rios, C. G. Moutinho, F. C. Pinto, F. S. Del Fiol, A. Jozala, M. V. Chaud, M. M. Vila, J. A. Teixeira and V. M. Balcao, *Microbiol. Res.*, 2016, **191**, 51–80.
30 M. R. Yeaman and N. Y. Yount, *Pharmacol. Rev.*, 2003, **55**, 27–55.
31 J. M. Sierra, E. Fusté, F. Rabanal, T. Vinuesa and M. Viñas, *Expert Opin. Biol. Ther.*, 2017, **17**, 663–676.
32 H. Lee, B. P. Lee and P. B. Messersmith, *Nature*, 2007, **448**, 338–341.
33 G. P. Maier, M. V. Rapp, J. H. Waite, J. N. Israelachvili and A. Butler, *Science*, 2015, **349**, 628–632.
34 J. H. Ryu, P. B. Messersmith and H. Lee, *ACS Appl. Mater. Interfaces*, 2018, **10**, 7523–7540.
35 J. Liebscher, R. Mrowczynski, H. A. Scheidt, C. Filip, N. D. Hadade, R. Turcu, A. Bende and S. Beck, *Langmuir*, 2013, **29**, 10539–10548.
36 M. d'Ischia, A. Napolitano, V. Ball, C. T. Chen and M. J. Buehler, *Acc. Chem. Res.*, 2014, **47**, 3541–3550.
37 J. Yang, M. A. Cohen Stuart and M. Kamperman, *Chem. Soc. Rev.*, 2014, **43**, 8271–8298.
38 J. Yu, Y. Kan, M. Rapp, E. Danner, W. Wei, S. Das, D. R. Miller, Y. Chen, J. H. Waite and J. N. Israelachvili, *Proc. Natl. Acad. Sci. U. S. A.*, 2013, **110**, 15680–15685.
39 S. A. Mian, L. M. Yang, L. C. Saha, E. Ahmed, M. Ajmal and E. Ganz, *Langmuir*, 2014, **30**, 6906–6914.
40 D. Song, L. Chen, T. Li and Z. R. Xu, *Colloids Interface Sci. Commun.*, 2021, **40**, 100340.
41 X. Chen, Y. Gao, Y. Wang and G. Pan, *Smart Mater. Med.*, 2021, **2**, 26–37.
42 Y. Xiao, W. Wang, X. Tian, X. Tan and Z. Yang, *Research*, 2020, **2020**, 1–12.
43 J. Bai, H. Wang, H. Chen, G. Ge and D. Geng, *Biomaterials*, 2020, **255**, 120197.
44 Y. Yang, P. Gao, J. Wang, Q. Tu, L. Bai, K. Xiong, H. Qiu, X. Zhao, M. F. Maitz, H. Wang, X. Li, Q. Zhao, Y. Xiao, N. Huang and Z. Yang, *Research*, 2020, **2020**, 9203906.
45 Y. Liu, K. Ai and L. Lu, *Chem. Rev.*, 2014, **114**, 5057–5115.
46 T. K. Das, S. Ganguly, S. Ghosh, S. Remanan and N. C. Das, *Colloids Interface Sci. Commun.*, 2019, **33**, 100218.
47 D. P. Griffith, D. M. Musher and C. Itin, *Invest. Urol.*, 1976, **13**, 346–350.
48 F. Atmani and S. R. Khan, *Urol. Res.*, 1995, **23**, 95–101.
49 O. Miyake, T. Yoshioka, K. Yoshimura, M. Honda, S. Yamaguchi, T. Koide and A. Okuyama, *Br. J. Urol.*, 1998, **81**, 14–19.
50 N. Shahkaramipour, T. N. Tran, S. Ramanan and H. Lin, *Membranes*, 2017, **7**, 13.
51 D. J. Miller, D. R. Dreyer, C. W. Bielawski, D. R. Paul and B. D. Freeman, *Angew. Chem., Int. Ed.*, 2017, **56**, 4662–4711.
52 J. Long, B. Teng, W. Zhang, L. Li, M. Zhang, Y. Chen, Z. Yao, X. Meng, X. Wang, L. Qin and Y. Lai, *Biomater. Transl.*, 2021, 272–284.

